SYNCHROSQUEEZING TRANSFORM AND ITS APPLICATIONS IN SEISMIC DATA ANALYSIS

WEI LIU[1,2], SIYUAN CAO[1,2], YANG LIU[1,2] and YANGKANG CHEN[3]

[1] *State Key Laboratory of Petroleum Resources and Prospecting, China University of Petroleum (Beijing), 18 Fuxue Road, Changping, Beijing 102249, P.R. China. liuwei_upc@126.com*
[2] *CNPC Key Laboratory of Geophysical Exploration, China University of Petroleum (Beijing), 18 Fuxue Road, Changping, Beijing 102249, P.R. China. csy@cup.edu.cn*
[3] *Bureau of Economic Geology, John A. and Katherine G. Jackson School of Geosciences, The University of Texas at Austin, University Station, Box X, Austin, TX 78713-8924, U.S.A. ykchen@utexas.edu*

(Received April 10, 2015; revised version accepted October 18, 2015)

ABSTRACT

Liu, W., Cao, S., Liu, Y. and Chen, Y., 2016. Synchrosqueezing transform and its applications in seismic data analysis. *Journal of Seismic Exploration*, 25: 27-44.

Time-frequency representation has been widely used in seismic data analysis because it can reveal a lot of information hidden in the seismic amplitude profiles. The short-time Fourier transform and wavelet transform are two popular methods to decompose a signal from time domain to time-frequency domain. However, the applications of both approaches are limited due to the trade-offs between time and frequency resolutions. The synchrosqueezing transform (SST) is a wavelet-based time-frequency reassignment method, which can produce an improved time-frequency resolution. In this paper, we extend the application of SST to hydrocarbon detection, ground roll suppression and random noise attenuation. In hydrocarbon detection, the SST shows high resolution in both time and frequency dimensions than continuous wavelet transform (CWT), which facilitates a better delineation of the location of low-frequency anomalies more clearly. In ground roll suppression, the SST performs better than the commonly used high-pass filtering and f-k filtering which damages the seismic reflections more or less. In random noise attenuation, the SST can be significantly more effective in both the removal of random noise and the preservation of useful reflection events compared with f-x deconvolution.

KEY WORDS: synchrosqueezing transform, hydrocarbon detection, ground roll suppression, random noise attenuation, continuous wavelet transform.

0963-0651/16/$5.00

INTRODUCTION

Time-frequency decomposition maps a 1D signal in the time domain into 2D image in time-frequency domain, which can characterize the local time-frequency properties and instantaneous frequency. As a powerful tool for the analysis of seismic data, time-frequency decomposition has been widely used in seismic data processing and interpretation. A widely used approach of time-frequency decomposition is the short-time Fourier transform (STFT) (Allen, 1977) which generates a localized time-frequency representation of a time series by applying the Fourier transform over a chosen time window (Gabor, 1946). However, the predefined window length limits the time-frequency resolution of STFT (Cohen, 1995). An alternative is the wavelet transform (WT) which applies the Fourier transform in small window to achieve a local time-frequency representation (Chakraborty et al., 1995). Unfortunately, a single scale encompasses a frequency band and is inversely proportional to the time support of the dilated wavelet. Moreover, it cannot be directly compared with other local time-frequency analysis methods. The S transform (Stockwell et al., 1996) is a combination of STFT and WT, it not only eliminates extra requirement of fixed window length for STFT but also is characterized by multi-resolution analysis of WT. Wigner-Ville distribution (Jeffrey, 1999; Wu et al., 2010) and Cohen distribution (Cohen, 1966) have higher time-frequency resolution, but the existence of interference or the cross-product terms limits their application. Matching pursuit (Mallat, 1993; Wang, 2007; Zhang et al., 2010) is another time-frequency analysis method which obtains time-frequency representation by decomposing a seismic trace into a series of wavelets that match its time-frequency signature. Despite its higher time-frequency resolution, it suffers from the expense of huge computational cost due to the redundancy of atom library. Portniaguine and Castagna (2004) described seismic signal spectral decomposition as an inverse problem, which produces solutions with better time and frequency resolution. Yuan and Wang (2013) proposed a sparse Bayesian learning reflectivity inversion in the Fourier domain to produce a super-resolution reflectivity, which can be used to effectively detect the boundaries of layers. Han and van der Baan (2013) presented the instantaneous spectra combined with Empirical Mode Decomposition (EMD), which facilitates the interpretation of reservoir thickness.

Synchrosqueezing transform (SST) (Daubechies et al., 2011) is an approach originally introduced in the context of audio signal analysis (Daubechies, 1996). It is a wavelet-based time-frequency representation and has a firm theoretical foundation. Meanwhile, the SST is also an adaptive and invertible transform that improves the readability of a wavelet-based time-frequency map (Li and Liang, 2012). Li and Liang (2012) proposed a generalized SST and it was used to extract a simulated gearbox fault signature from a noisy signal and detect gearbox faults. Meignen (2012) presented a novel algorithm based on SST and applied it to sampling and denoising of

multicomponent signals. Thakur et al. (2013) implemented SST to examine characteristics of a key paleoclimate change in the last 2.5 million years, which contributes to our understanding of the link between solar forcing and climate response on very long time scales. Herrera (2014) employed SST to depict amplitude variations of channel and fault on horizontal slices, which is helpful to calculate subtle thickness variations. Wang (2014) introduced SST to the channel and subtle fault characterization which is helpful in more accurately locating the various reflections and facilitating further interpretation. Chen (2014) applied SST to detecting anomalies of high-frequency attenuation and deep-layer weak signal. Herrera (2015) utilized SST to achieve the separation and identification of P- and S-waves with subtly different frequency contents in the time-frequency domain. Chen (2015) applied SST in delineating the karstification of the Boonsiville field, Texas.

In this paper, we show the further application of SST in seismic data analysis including hydrocarbon detection, ground roll suppression and random noise attenuation. The paper is arranged as follows: the theory of SST and the principles of hydrocarbon detection, ground roll suppression and random noise attenuation are introduced in the second section. In the next section, we utilize a non-stationary synthetic example to show the high resolution of SST in both time and frequency compared with CWT. In order to further demonstrate the applicability of SST in the seismic data processing and interpretation, field data examples are also presented. The advantage of SST is highlighted in comparison with CWT in hydrocarbon detection. For ground roll suppression, we make a comparison between the SST and other two conventional approaches. Then the SST and f-x deconvolution are used to attenuate random noise and their performances are evaluated. The last section presents the conclusions which indicate that the SST is a promising tool for time-frequency analysis, including hydrocarbon detection, ground roll removal and random noise attenuation.

THEORY

Synchrosqueezing transform

The CWT is defined as the inner product of the family of wavelet $\psi_{a,b}(t)$ with the signal f(t), which can be formulated as

$$\begin{aligned} W_f(a,b) &= \langle f(t), \psi_{a,b}(t) \rangle \\ &= \int_{\infty}^{-\infty} f(t)(1/\sqrt{a})\psi^*[(t-b)/a]dt \quad , \end{aligned} \tag{1}$$

where ψ^* is the complex conjugate of ψ, b is the time shift and a is the dilation

parameter or scale. $W_f(a,b)$ are the wavelet transform coefficients representing a concentrated time-frequency map, which is used to extract the instantaneous frequency (Daubechies et al., 2011).

Daubechies et al. (2011) found that there is a physical limit to reduce the smearing effect in the time-frequency representation by the CWT. According to Plancherel's theorem (energy in the time domain equals energy in the frequency domain), eq. (1) can be rewritten as:

$$W_f(a,b) = (1/2\pi) \int (1/\sqrt{a})\hat{f}(\xi)\hat{\psi}^*(a\xi)e^{jb\xi}d\xi \quad , \tag{2}$$

where ξ represents frequency, and $\hat{\psi}(\xi)$ is the Fourier transform of $\xi(t)$. Besides, the frequency of the wavelet ξ is modified by the scale a. Also, b is represented by its Fourier pair $e^{jb\xi}$.

In the frequency dimension, if the wavelet $\hat{\psi}^*(\xi)$ is concentrated around its central frequency $\xi = \omega_0$, then $W_f(a,b)$ will be concentrated around the scale $a = \omega_0/\omega$ (the ratio of the central frequency of the wavelet to the central frequency of the signal). However, the wavelet transform $W_f(a,b)$ often spreads out over a region around the scale $a = \omega_0/\omega$ on the time-scale dimension. If the smearing along the time dimension can be neglected (Daubechies and Maes, 1996), the instantaneous frequency $\omega_f(a,b)$ can be computed as:

$$\omega_f(a,b) = -j[W_f(a,b)]^{-1}(\partial/\partial b)W_f(a,b) \quad . \tag{3}$$

The information from the time-scale dimension is transferred to time-frequency domain because the (b,a) is converted to $[b,\omega_f(a,b)]$. $W_f(a,b)$ is computed only at discrete values a_k, with $a_k - a_{k-1} = Va_k$, and its synchrosqueezed transform $T_f(\omega,b)$ is determined only at the centres ω_l of the frequency range $[(\omega_l - V\omega/2),(\omega_l + V\omega/2)]$ with $\omega_l - \omega_{l-1} = V\omega$:

$$T_f(\omega_l,b) = (V\omega)^{-1} \sum_{a_k:|\omega(a_k,b)-\omega_l| \le V\omega/2} W_f(a_k,b)a_k^{-3/2}Va_k \quad . \tag{4}$$

Eq. (4) shows that the new time-frequency representation $T_f(\omega_l,b)$ is only synchrosqueezed along the frequency axis (Li and Liang, 2012).

The SST is invertible and the reconstruction of the original signal from the synchrosqueezed transform $T_f(\omega_l,b)$ can be expressed as:

$$f(b) = \Re e[C_\psi^{-1} \int_0^\infty W_f(a,b)a^{-3/2}da]$$

$$\approx \Re e[C_{\psi}^{-1} \sum_{k} W_f(a_k,b) a_k^{-3/2} \Delta a_k]$$

$$= \Re e[C_{\psi}^{-1} \sum_{l} T_f(\omega_l,b) \Delta\omega] \quad . \tag{5}$$

where $C_{\psi} = \frac{1}{2} \int_0^{\infty} \hat{\psi}^*(\xi)(d\xi/\xi)$ and C_{ψ} is dependent on the selected wavelet.

Instantaneous spectral analysis

The high-frequency components of seismic waves decays rapidly as seismic waves propagate due to the presence of oil and gas, which results in low-frequency shadows on seismic section. This low-frequency anomaly is usually employed to detect hydrocarbon reservoir, for which the accuracy of time-frequency decomposition is vitally important. The SST provides good time-frequency resolution and is therefore effective in detecting low-frequency shadows caused by hydrocarbon reservoir. We use the Morlet mother wavelet to perform time-frequency decomposition based on eq. (4), and then the instantaneous spectra are extracted to exhibit the low-frequency anomaly associated with hydrocarbon reservoir.

Time-frequency filtering with the SST

Time-frequency filter has been widely applied to attenuate the ground roll components (Askari and Siahkoohi, 2008). According to the information obtained from the SST of seismic data, we can design an effective time-frequency filter. This process can be expressed as:

$$y(t) = SST^{-1}\{SST[f(t)]H(t,f)\} \quad , \tag{6}$$

where SST and SST^{-1} denote synchrosqueezing transform and inverse synchrosqueezing transform, respectively. H(t,f) is the time-frequency filter, which generally is designed as eq. (7) based on the difference between seismic signals and ground roll in time-frequency map.

$$H(t,f) = \begin{cases} 1 & f \in [f_i(t) - B(t)/2,\ f_i(t) + B(t)/2] \\ 0 & \text{others} \end{cases} \quad , \tag{7}$$

where $f_i(t)$ is the instantaneous frequency of seismic signals, B(t) is the bandwidth of time-frequency filter.

Threshold denoising

The wavelet threshold denoising algorithm has been adopted as a successful method, which has several merits such as convenient and efficient calculation and better performance for components with low SNR. In the paper, eq. (8) is served as threshold function to attenuate random noise combined with the SST.

$$\hat{\mathbf{S}}_{t,f} = \begin{cases} \mathrm{sgn}(\mathbf{S}_{t,f})(|\mathbf{S}_{t,f}| - \alpha\lambda) & |\mathbf{S}_{t,f}| \geq \lambda \\ 0 & |\mathbf{S}_{t,f}| < \lambda \end{cases}, \tag{8}$$

where α determines the threshold function type: hard threshold ($\alpha = 0$) or soft threshold ($\alpha = 1$). λ denotes the threshold and is expressed as:

$$\lambda = \sqrt{(2\log n)}\ \sigma_n \ , \tag{9}$$

where n is the number of time samples and σ_n is the noise standard deviation and can be estimated by (Herrera, 2014):

$$\sigma_n = 1.4826\,\mathrm{median}\{|W_f(a_{1:n_v},b) - \mathrm{median}[W_f(a_{1:n_v},b)]|\} \ , \tag{10}$$

where $W_f(a_{1:n_v},b)$ are the wavelet coefficients at finest scale and 1.4826 is a normalizing factor.

EXAMPLES

Synthetic data

In order to demonstrate the effectiveness of SST in seismic data analysis, we first test the SST with a non-stationary synthetic signal (Fig. 1). For comparison, the time-frequency representation based on CWT is also applied to this data. This signal is comprised of a constant 20 Hz sine wave from 0 to 1s, a 10 Hz cosine wave from 1 to 2 s, a 100 Hz Morlet wavelet at 0.6 s, a 45 Hz zero-phase Ricker wavelet at 1.4 s and a 70 Hz 180° phase shifted Ricker wavelet at 1.8 s.

Both CWT and SST are applied to the synthetic data, respectively. Time-frequency representations based on CWT and SST are shown in Figs. 2(a) and 2(b), respectively. It can be seen that the CWT can reveal all components in synthetic signal but the time-frequency resolution is poor especially for the frequency resolution of the Morlet wavelet and two Ricker wavelets. In contrast, the SST shows an enhanced time-frequency resolution. It is also obvious that the SST produces sparse time-frequency map and all components in the synthetic signal are depicted well compared with CWT.

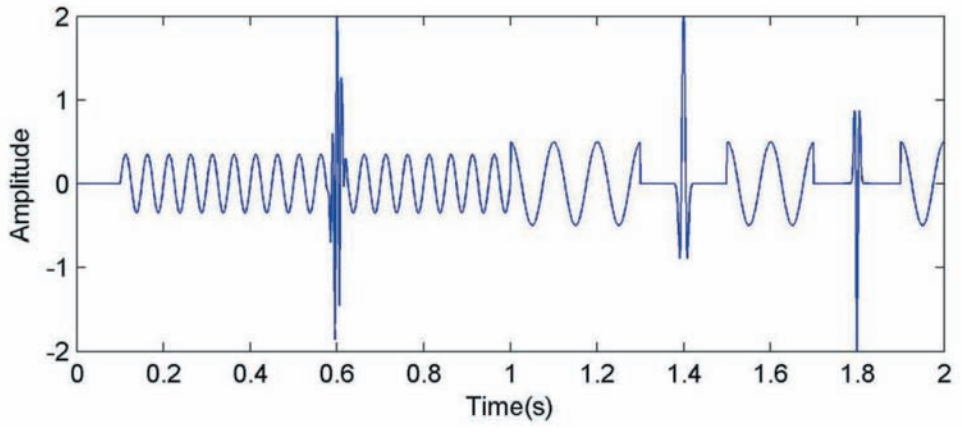

Fig. 1. Synthetic example: 20 Hz sine wave from 0 to 1 s, 10 Hz cosine wave from 1 to 2 s, 100 Hz Morlet wavelet at 0.6 s, 45 Hz Ricker wavelet at 1.4 s and 70 Hz Ricker wavelet at 1.8 s.

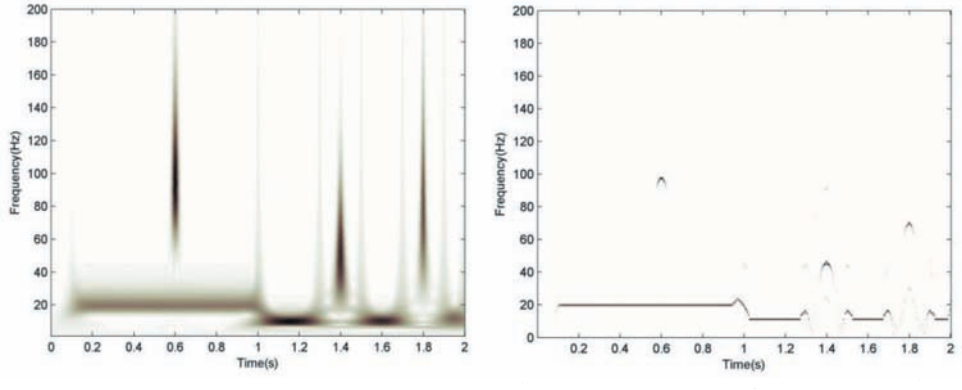

a b

Fig. 2. Time-frequency representation of the synthetic data. (a) CWT result, note that the frequency resolution is poor, especially for the Morlet wavelet at 0.6 s, the Ricker wavelets at 1.4 s and 1.8s. (b) SST result, showing an enhanced time and frequency resolution.

Fig. 3(a) shows the reconstructed signal from SST, from which it can be observed that the SST has a perfect reconstruction. The reconstruction error is shown in Fig. 3(b). It is obvious that the reconstruction error is very close to zero.

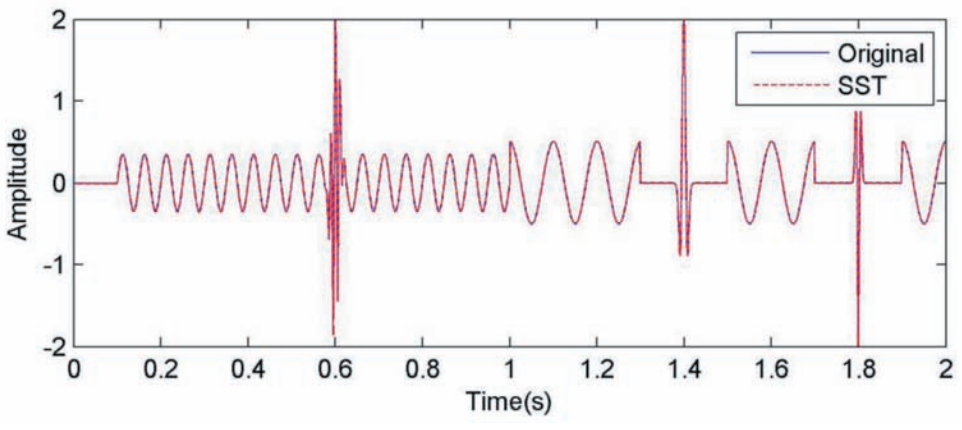

a

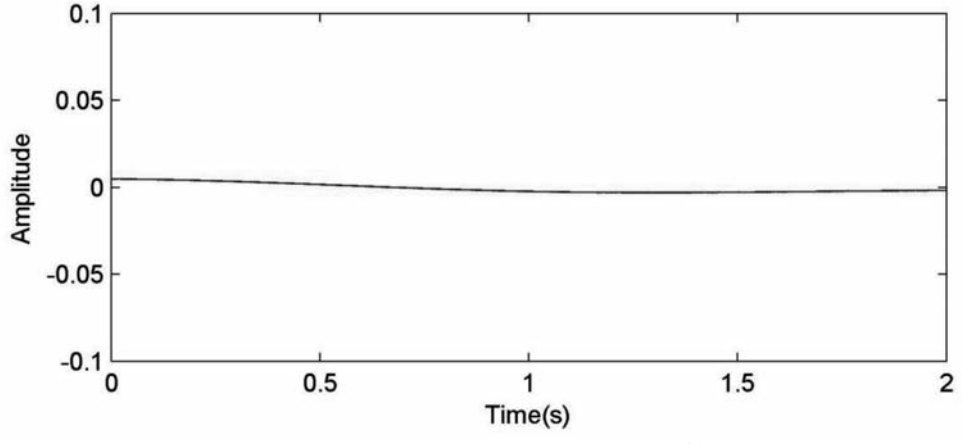

b

Fig. 3. Reconstructed signal (a) and reconstruction error (b). Note that there is no observable difference between reconstructed signal and original signal, and the reconstruction error is approximately zero.

Hydrocarbon detection

In this section, we apply the SST to a field data and compare the performance with that of the CWT. Fig. 4 is real seismic data that shows bright amplitude (white ellipse), indicating a known hydrocarbon zone. We take the trace No. 20 shown in Fig. 5 as a single-trace example. The time-frequency

representations corresponding to CWT and SST are shown in Fig. 6. It can be seen that both of them indicate the strong low-frequency anomaly, but the SST exhibits a sparser image and cleaner representation owing to the higher time-frequency resolution.

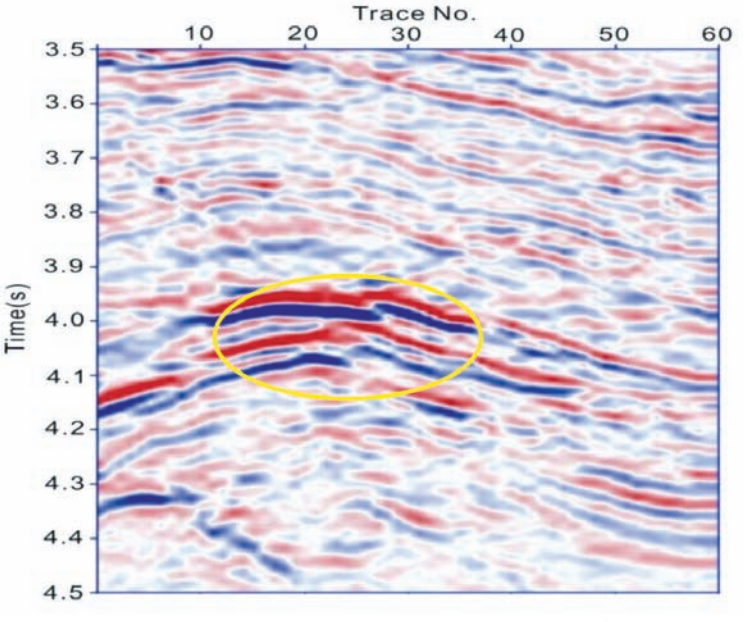

Fig. 4. Real seismic data. Bright amplitudes indicated by a white ellipse is a known hydrocarbon zone.

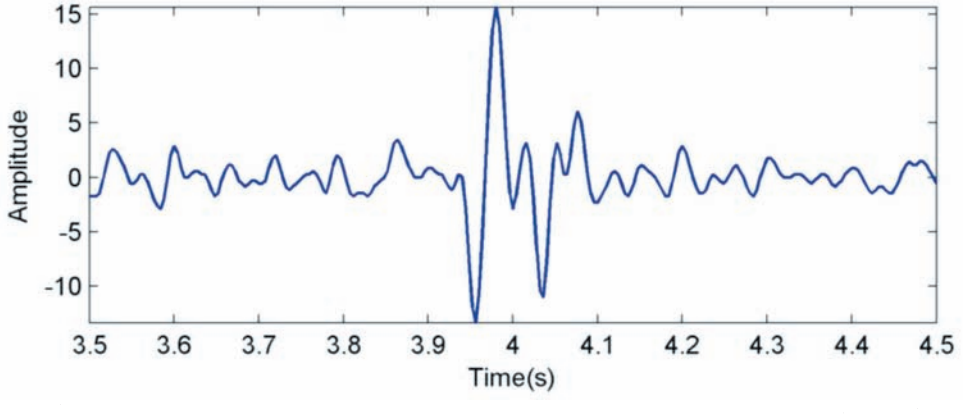

Fig. 5. Individual trace at No. 20 in Fig. 4.

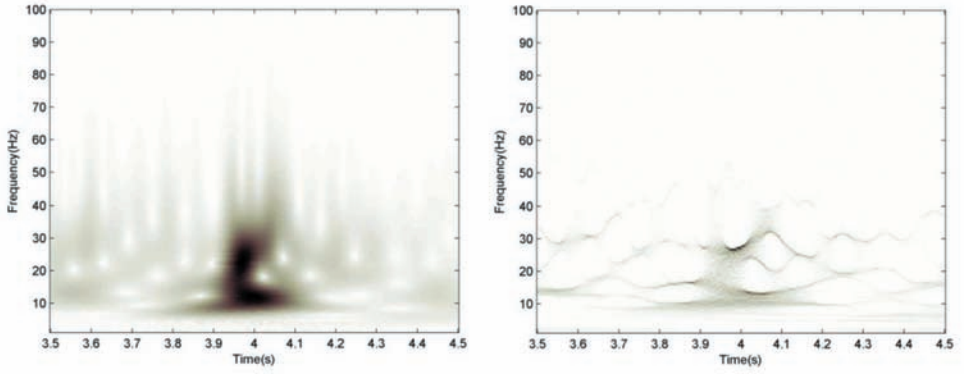

Fig. 6. No. 20 time-frequency representation from (a) CWT and (b) SST. Both of them indicate the strong low-frequency anomaly around 4.0 s, but the SST result shows much clearer delineation.

Figs. 7(a) and 7(b) show the frequency slices from the CWT with frequencies of 25 Hz and 40 Hz, respectively. Figs. 7(c) and 7(d) show the corresponding frequency slices from the SST. The target area has been proved to contain gas by exploiting the well.

As we see from Fig. 7, both low-frequency slices exhibit high-amplitude anomalies (yellow ellipse and white arrow), but the frequency slices from the SST provide much higher resolution compared with CWT, which is helpful in detecting the location of anomaly more clearly, thus facilitating further interpretation.

Ground roll suppression

Ground roll is a source-generated surface wave whose vertical component is composed of dispersive Rayleigh waves whose different frequency components have different velocities (Bereford-Smith and Rango, 1988). On seismic records, the ground roll often interferes with seismic data and overlays the useful reflections. Commonly used processing techniques for attenuating ground roll mainly include frequency filtering, and f-k filtering.

We applied the SST to a real shot gather contaminated by ground roll (Fig. 8) and designed a filter based on eq. (7) to suppress the ground roll components localized in both time and frequency domain. Then, the shot gather

after denoising is reconstructed by the inverse SST. Comparisons are made between the results of the SST, high-pass filtering and f-k filtering to evaluate the effect of the SST. The denoised shot gather and its difference with the original shot gather are indicated in Figs. 9(a) and 9(b). As seen in Fig. 9, the ground roll is suppressed effectively and the signals underlying the ground roll are well recovered. The shot gathers after high-pass filtering and f-k filtering are shown Figs. 10(a) and 11(a), respectively. Their differences with the original shot gather are indicated in Figs. 10(b) and 11(b), respectively.

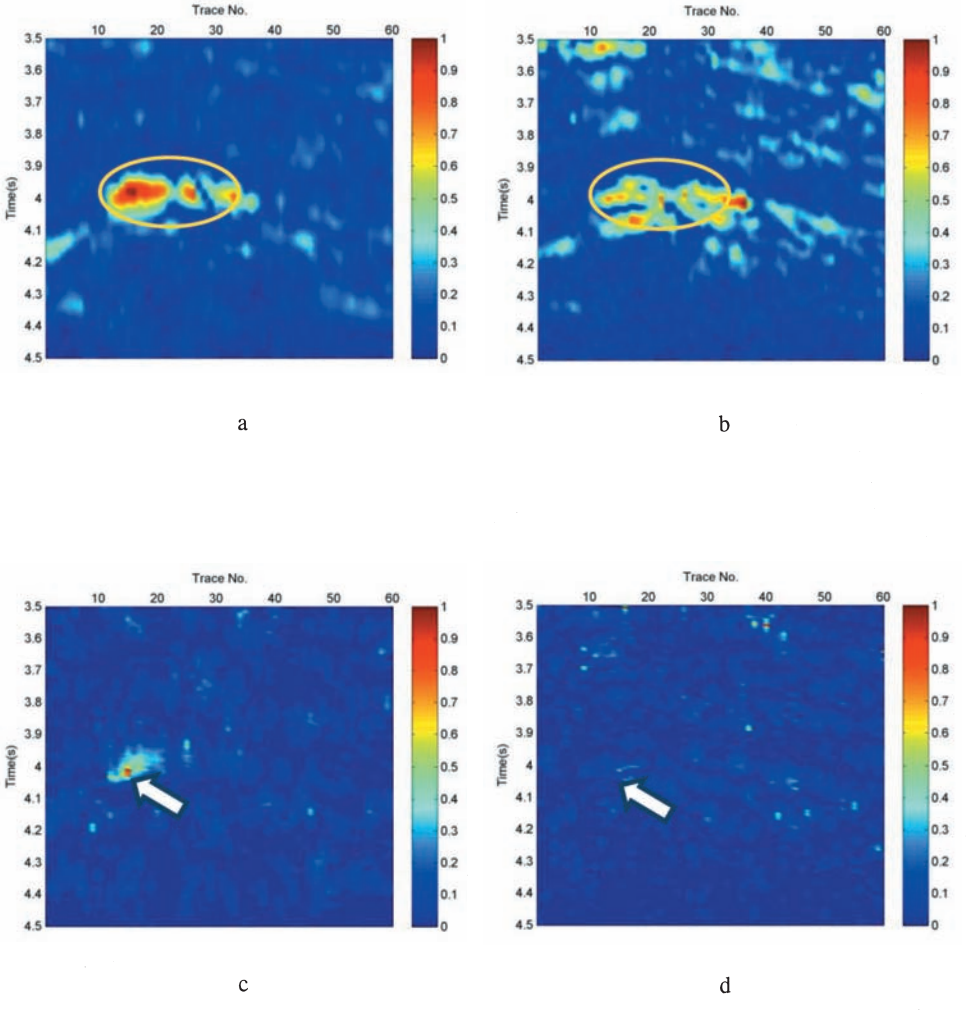

Fig. 7. Frequency slices for gas indication. (a) CWT spectrum at 25 Hz, (b) CWT spectrum at 40Hz, (c) SST spectrum at 25 Hz and (d) SST spectrum at 40 Hz. The SST shows a sparser representation than the CWT, which might potentially help locate the reservoir with higher accuracy.

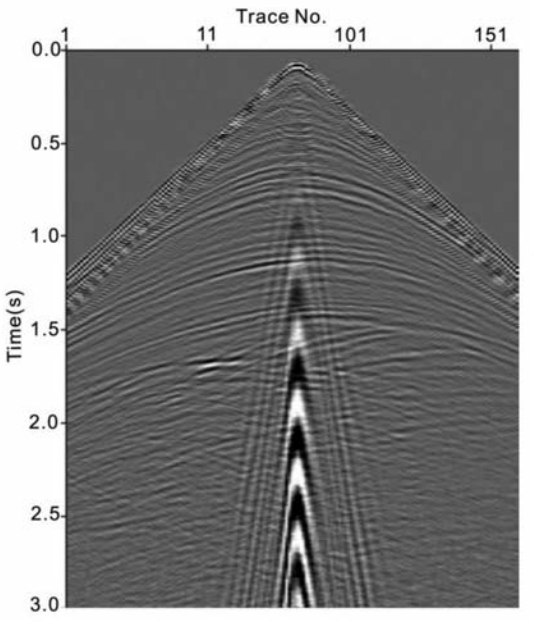

Fig. 8. A seismic shot gather contaminated with ground roll.

From Figs. 9(a), 10(a) and 11(a), it can be observed that all the three approaches can suppress the ground roll well. However, comparison of Figs. 9(b), 10(b) and 11(b) indicates that almost no seismic reflection has been removed using the SST. It works better than high-pass filtering and f-k filtering, which damage the useful seismic reflections more or less.

Fig. 12 shows the time-frequency representation of trace 80 before and after ground roll suppression with SST. The box in Fig. 12(a) covers an area corresponding to the time-frequency representation of the ground roll. Fig. 12(b) indicates that the time-frequency spectrum of seismic reflection is more obvious after ground roll suppression.

Random noise attenuation

Random noise attenuation plays an important role in seismic data processing for enhancing the seismic reflections and reduce the interpretation risks (Chen and Ma, 2014; Chen and Fomel, 2015). In this paper, we propose to use the time-frequency analysis approach for separating the useful seismic signals and random noise. The difference between the useful signals and noise is more obvious in time-frequency domain because of a higher time-frequency resolution of the SST. Thus, the SST is used to attenuate random noise in seismic data.

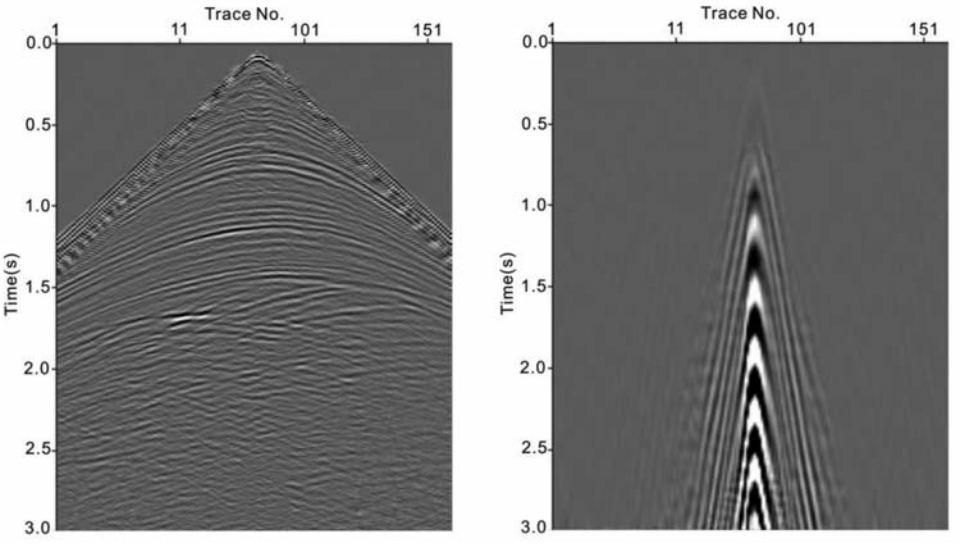

a b

Fig. 9. Ground roll attenuation. (a) Denoised shot gather using SST; (b) its difference with the original shot gather.

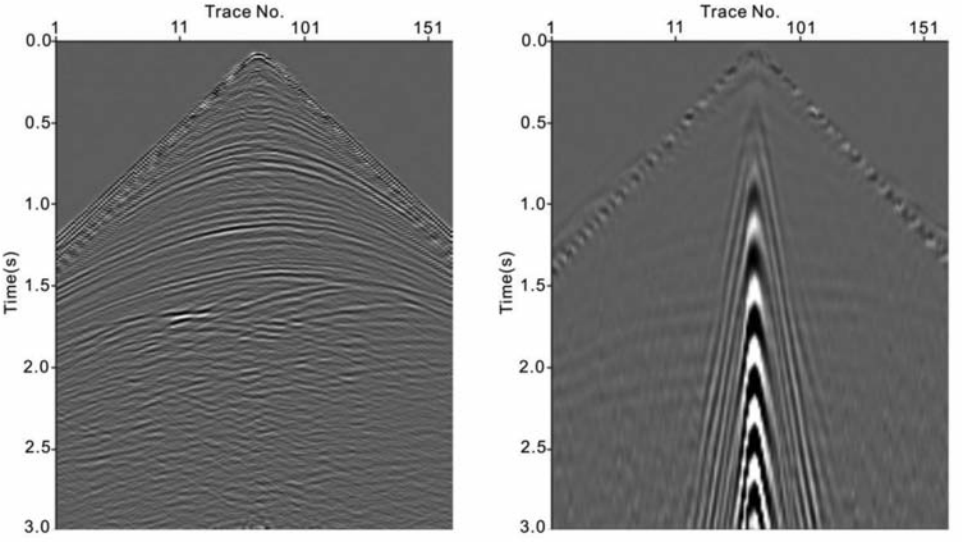

a b

Fig. 10. Ground roll attenuation. (a) Denoised shot gather using high-pass filter; (b) its difference with the original shot gather.

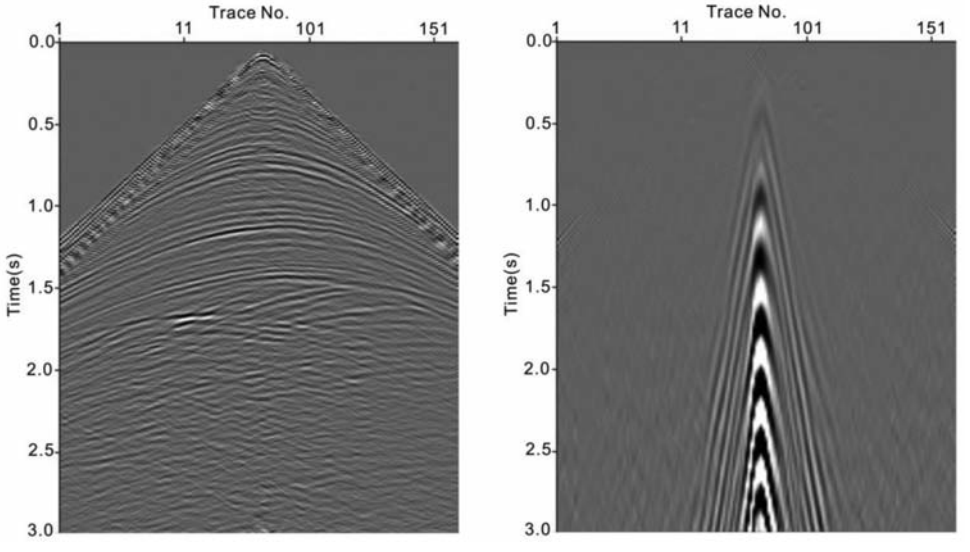

a b

Fig. 11. Ground roll attenuation. (a) Denoised shot gather using f-k filter; (b) its difference with the original shot gather.

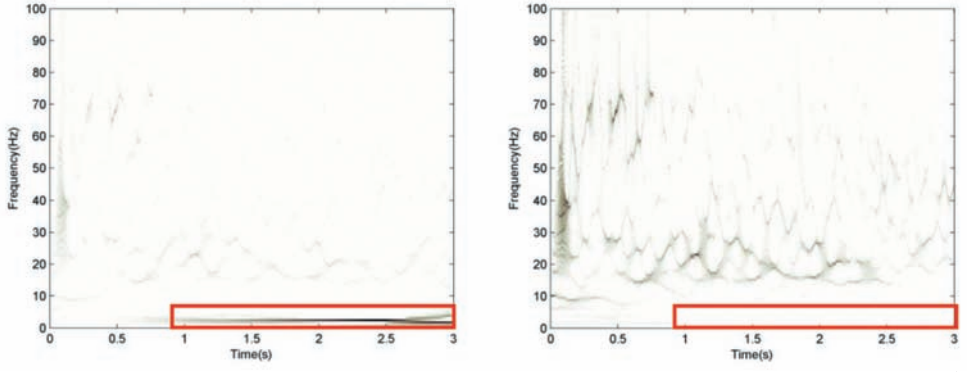

a b

Fig. 12. (a) Time-frequency representation of trace 80, the box covers an area corresponding to the ground roll. (b) Time-frequency representation of trace 80 after the ground roll attenuation.

Fig. 13 is a seismic record contaminated with random noise which has 1000 traces, 321 sampling points, the time sampling interval of 2 ms. For comparison, the commonly used f-x deconvolution (Canales, 1984; Yang and Wang, 2011) is also applied to this data. As seen in Fig. 13, the SNR of seismic data is low due to the presence of noise, and the continuity of seismic events is poor, which makes the interpretation and evaluation of the reflection events difficult. After using SST and f-x deconvolution, we obtain denoised seismic data that are shown in Figs. 14(a) and 14(c), respectively. Figs. 14(b) and 14(d) show the difference between the denoised data and original data, respectively. From the denoising performance, it is evident that the SST can suppress most of the noise effectively and the signals underlying the random noise are recovered well, the seismic data becomes clearer and seismic reflections become more continuous, which is beneficial for the following processing and interpretation. In addition, there are nearly no effective reflections in the removed noise section [Fig. 14(b)]. In contrast, although the f-x deconvolution can also attenuate random noise well, it seems to damage some effective reflections to some extent, which can be found in the removed noise section using f-x deconvolution [Fig. 14(d)].

Fig. 15 shows the time-frequency representation of trace 500 before and after random noise attenuation with SST. It can be seen that the random noise is effectively attenuated, meanwhile, the seismic reflections are highlighted.

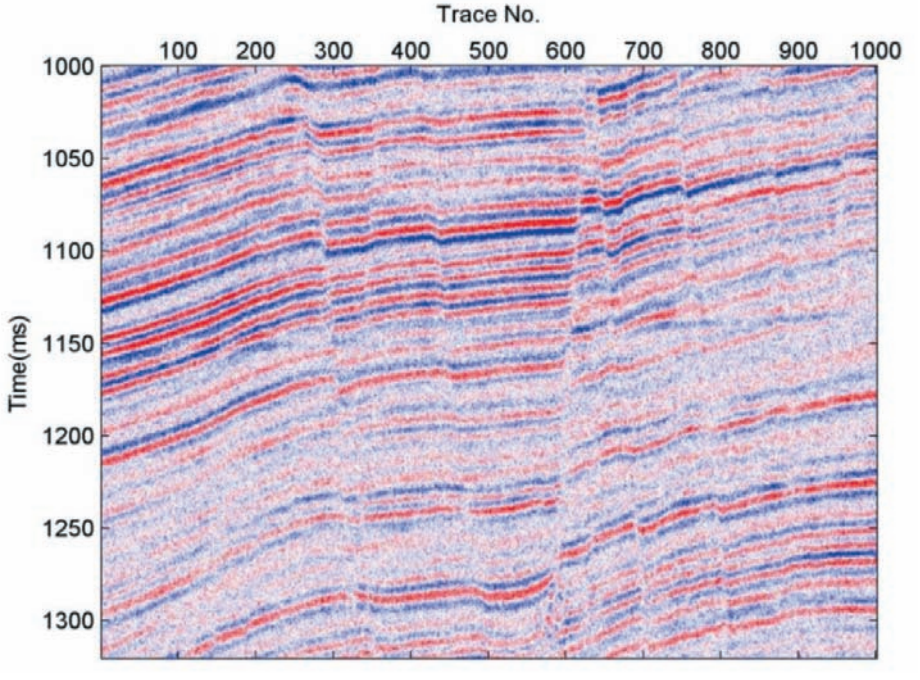

Fig. 13. Real seismic data with random noise.

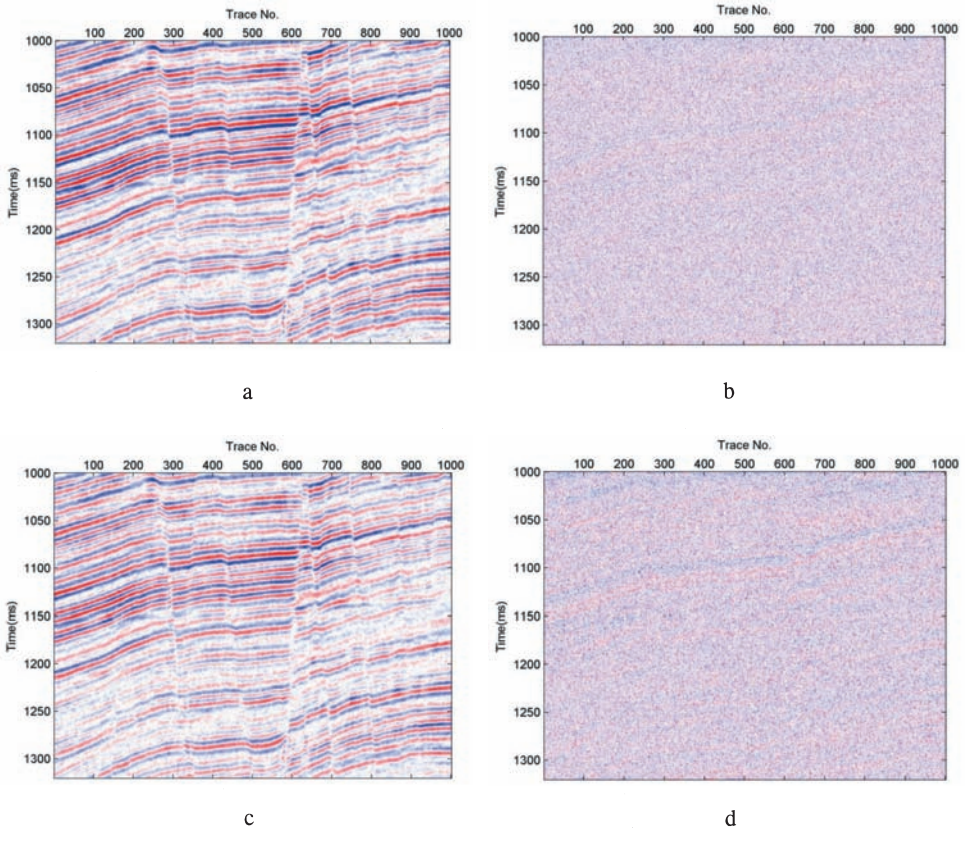

Fig. 14. Random noise attenuation. (a) Denoised seismic record using SST; (b) Removed noise for SST; (c) Denoised seismic record using f-x deconvolution; (d) Removed noise for f-x deconvolution.

CONCLUSIONS

The SST is mathematically formulated and invertible, which makes it able to provide a more robust time-frequency analysis than those EMD based approaches and to reconstruct signal from the time-frequency domain in order to remove some types of noise in the seismic data according to the time-frequency difference between noise and useful signals. We have introduced the SST with several applications to seismic data analysis, which shows promising results in both synthetic data and field data. The synthetic example shows higher time-frequency resolution compared with CWT. The field data examples indicate that the SST can be applied to detect hydrocarbon reservoir, suppress ground roll and attenuate random noise. We find that the SST is more helpful in delineating the location of seismic reflections more accurately compared with CWT. The SST works better than the high-pass filtering and f-k filtering in ground roll suppression. The SST can not only attenuate the random

noise well, but also can preserve more useful reflections compared with the commonly used f-x deconvolution.

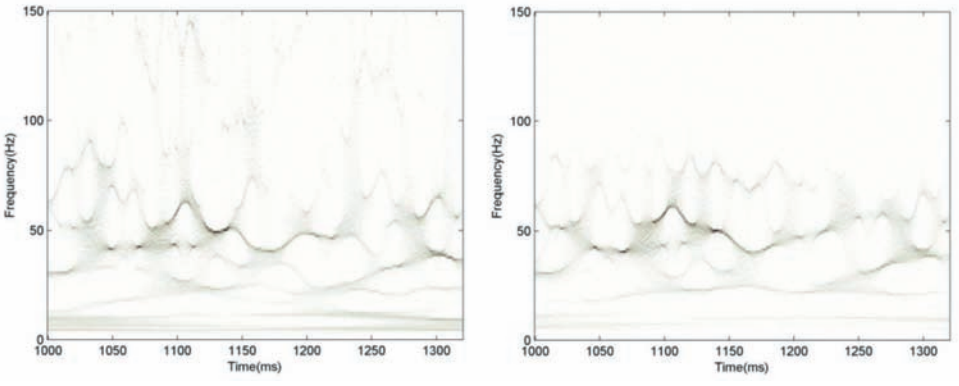

Fig. 15. (a) Time-frequency representation of trace 500 before random noise attenuation; (b) Time-frequency representation of trace 500 after random noise attenuation using SST. The seismic reflections are highlighted after random noise attenuation.

ACKNOWLEDGMENTS

This work is financially supported by the National Science and Technology Major Project of China under Grants No. 2011ZX05024-001-01. Yangkang Chen is supported by the Texas Consortium for Computational Seismology. We would like to thank Ron Gramende, Summer Li, Zhaoyu Jin, and anonymous reviewers for suggestions and comments that have greatly improved the manuscript. Moreover, we are also grateful for the support of the Australian and Western Australian Governments and the North West Shelf Joint Venture Partners, as well as the Western Australian Energy Research Alliance.

REFERENCES

Allen, J.B., 1977. Short term spectral analysis, synthetic and modification by discrete fourier transform. IEEE Trans. Acoust. Speech Sign. Process., 25: 235-238.

Askari, R. and Siahkoohi, H.R., 2008. Ground roll attenuation using the S and x-f-k transform. Geophys. Prosp., 56: 105-114.

Beresford-Smith, G. and Rango, R., 1988. Dispersive noise removal in t-x space: Application to Arctic data. Geophysics, 53: 346-358.

Canales, L., 1984. Random noise reduction. Expanded Abstr., 54th Ann. Internat. SEG Mtg., Atlanta: 525-527.

Chakraborty, A. and Okaya. D., 1995. Frequency-time decomposition of seismic data using wavelet-based method. Geophysics, 60: 1906-1916.

Chen, Y., Liu, T., Chen, X. and Wang, E., 2014. Time-frequency analysis of seismic data using synchrosqueezing wavelet transform. Expanded Abstr., 84th Ann. Internat. SEG Mtg., Denver: 1589-1592.

Chen, Y. and Ma, J., 2014. Random noise attenuation by f-x empirical mode decomposition predictive filtering. Geophysics, 79: V81-V91.

Chen, Y. and Fomel, S., 2015. Random noise attenuation using local signal-and-noise orthogonalization. Geophysics, 80: WD1-WD9.

Chen, Y., Li, S.X., Zhang, G. and Gan, S., 2015. Delineating karstification using synchrosqueezing wavelet transform. Expanded Abstr., 85th Ann. Internat. SEG Mtg., New Orleans: in press.

Cohen, L., 1966. Generalized phase-space distribution functions. J. Math. Phys., 7: 781-786.

Cohen, L., 1995. Time-frequency Analysis. Prentice-Hall, New York.

Daubechies, I. and Maes, S., 1996. A nonlinear squeezing of the continuous wavelet transform based on auditory nerve models wavelets in medicine and biology. In: Aldroubi, A. and Unser, M. (Eds.), Wavelets in Medicine and Biology. CRC Press, Boca Raton: 527-546.

Daubechies, I., Lu, J. and Wu, H.T., 2011. Synchrosqueezed wavelet transform: An empirical mode decomposition-like tool. Appl. Comput. Harmon. Anal., 30: 243-261.

Gabor, D., 1946. Theory of communication. J. Inst. Electr. Engin., 93: 429-497.

Han, J. and van der Baan, M., 2013. Empirical mode decomposition for seismic time-frequency analysis. Geophysics, 78: 9-19.

Herrera, R.H., Han, J. and van der Baan. M., 2014. Applications of the synchrosqueezing transform in seismic time-frequency analysis. Geophysics, 79: V55-V64.

Herrera, R.H., Tary, J.B., van der Baan, M. and Eaton, D.W., 2015. Body wave separation in the time-frequency domain. IEEE Geosci. Remote Sens., 12: 364-368.

Jeffrey, C. and William, J., 1999. On the existence of discrete Wigner distributions. IEEE Signal Proc. Lett., 6: 304-306.

Li, C. and M. Liang., 2012. A generalized synchrosqueezing transform for enhancing signal time-frequency representation. Signal Process., 92: 2264-2274.

Li, C. and Liang, M., 2012. Time-frequency signal analysis for gearbox fault diagnosis using a generalized synchrosqueezing transform. Mech. Syst. Signal Process., 26: 205-217.

Mallat, S.G. and Zhang, Z.F., 1993. Matching pursuits with time frequency dictionaries. IEEE Trans. Signal Process., 41: 3397-3415.

Meignen, S., Oberlin, T. and McLaughlin, S., 2012. A new algorithm for multicomponent signals analysis based on synchrosqueezing: With an application to signal sampling and denoising. IEEE Trans. Signal Process., 61: 5787-5798.

Portniaguine, O. and Castagna, J., 2004. Inverse spectral decomposition. Expanded Abstr., 74th Ann. Internat. SEG Mtg., Denver: 1786-1789.

Stockwell, R.G., Mansinha, L. and Lowe, R.P., 1996. Localization of the complex spectrum: The S-transform. IEEE Trans. Signal Process., 44: 998-1001.

Thakur, G.E., Brevdo, N.S., Fuckar, N.S. and Wu, H.T., 2013. The synchrosqueezing algorithm for time-varying spectral analysis: Robustness properties and paleoclimate applications. Signal Process., 93: 1079-1094.

Wang, P., Gao, J. and Wang, Z., 2014. Time-frequency analysis of seismic data using synchrosqueezing transform. IEEE Geosci. Remote Sens., 11: 2042-2044.

Wang, Y., 2007. Seismic time-frequency spectral decomposition by matching pursuit. Geophysics, 72: V13-V20.

Wu, X.Y. and Liu, T.Y., 2010. Seismic spectral decomposition and analysis based on Wigner-Ville distribution for sandstone reservoir characterization in West Sichuan depression. Geophysics, 7: 126-134.

Yuan, S.Y. and Wang, S.X., 2011. A local f-x Cadzow method for noise reduction of seismic data obtained in complex formations. Petrol. Sci., 8: 269-277.

Yuan, S.Y. and Wang, S.X., 2013. Spectral sparse Bayesian learning reflectivity inversion. Geophys. Prosp., 61: 735-746.

Zhang, X., Han, L., Wang, Y. and Shan, G., 2010. Seismic spectral decomposition fast matching pursuit algorithm and its application. Geophys. Prosp. Petrol., 49: 1-6.